

THERMOACOUSTIC LIQUEFACTION - TOTAL BUDGET, AUD

Cost estimate (very approx)	ALL AUD			
	Getting started	Eliminate tech risk	Build and demonstrate	
ProjPlan	1,995,000	\$1,330,000	\$399,000	
1stStEng	\$1,795,500	\$1,330,000	\$1,995,000	
3-StgEng	\$465,500	\$1,363,250	\$5,320,000	
1st PTR	\$997,500	\$1,197,000	\$1,995,000	
All PTR	---	\$399,000	\$3,990,000	
CO2Clean	\$532,000	\$266,000	\$2,660,000	
Product removal	\$532,000	\$266,000	\$1,330,000	
Controls	\$133,000	\$266,000	\$997,500	
TestSite	\$900,000	\$133,000	\$1,330,000	
FullDemo	---	---	\$3,990,000	
Contingency			\$2,000,000	
Totals - in AUD:	\$ 7,350,500	\$ 6,550,250	\$ 26,006,500	\$ 39,907,250

SUBSCRIPTION

Federal Gov't 33.3%	2,450,167	2,183,417	8,668,833	13,302,417
---------------------	-----------	-----------	-----------	-------------------

PROFIT & LOSS STATEMENT FOR PUTAR CO₂ CAPTURE & SUPER CRITICAL PRESSURE PULSE COMBUSTION BOILER POWER STATIONS

case 1: EXISTING BROWN COAL POWER STATIONS

Item	income	expense
extra electricity produced from increased efficiency by using PUTAR (based on \$41.00 /MW-h, source NEMCO*)	\$16.40	
removal of CO ₂ from flue gas produced at 1.4t CO ₂ /MW-h with process costing \$6.00/t		\$8.40
selling CO ₂ @ \$5.00/t	\$7.20	
net PROFIT/MW-h	\$15.20	
removal of CO ₂ from flue gas produced at 1.4t CO ₂ /MW-h with process costing \$3.00/t		\$4.20
net PROFIT/MW-h	\$19.40	

* ave over 5 years for QLD, NSW, VIC & SA coal fired power stations

case 2: EXISTING BLACK COAL POWER STATIONS

Item	income	expense
extra electricity produced from increased efficiency by using PUTAR (based on \$41.00 /MW-h, source NEMCO)	\$16.40	
removal of CO ₂ from flue gas produced at 1.2t CO ₂ /MW-h with process costing \$6.00/t		\$7.20
selling CO ₂ @ \$5.00/t	\$7.20	
net PROFIT/MW-h	\$16.40	
removal of CO ₂ from flue gas produced at 1.2t CO ₂ /MW-h with process costing \$3.00/t		\$3.60
net PROFIT/MW-h	\$20.00	

case 3: IGCC (Brown Coal) & SCP PULSE COMBUSTION BOILER POWER STATIONS

Item	income	expense
extra electricity produced from increased efficiency by using SCP Pulse Combustion (based on \$41.00 /MW-h, source NEMCO)	\$20.50	
removal of CO ₂ from flue gas produced at 1.4t CO ₂ /MW-h with process costing \$6.00/t		\$8.40
selling CO ₂ @ \$5.00/t	\$7.20	
net PROFIT/MW-h	\$19.30	
removal of CO ₂ from flue gas produced at 1.4t CO ₂ /MW-h with process costing \$3.00/t		\$4.20
net PROFIT/MW-h	\$23.50	

case 4: NATURAL GAS SCP PULSE COMBUSTION BOILER POWER STATIONS

Item	income	expense
extra electricity produced from increased efficiency by using SCP Pulse Combustion (based on \$41.00 /MW-h, source NEMCO)	\$20.50	
removal of CO ₂ from flue gas produced at 0.7t CO ₂ /MW-h with process costing \$6.00/t		\$4.20
selling CO ₂ @ \$5.00/t	\$7.20	
net PROFIT/MW-h	\$23.50	
removal of CO ₂ from flue gas produced at 0.7t CO ₂ /MW-h with process costing \$3.00/t		\$2.10
net PROFIT/MW-h	\$25.60	

PROFIT & LOSS STATEMENT FOR PUTAR CO₂ CAPTURE & SUPER CRITICAL PRESSURE PULSE COMBUSTION BOILER POWER STATIONS

case 5: EXISTING BROWN COAL POWER STATIONS - No sale of CO₂

Item	income	expense
extra electricity produced from increased efficiency by using PUTAR (based on \$41.00 /MW-h, source NEMCO*)	\$16.40	
removal of CO ₂ from flue gas produced at 1.4t CO ₂ /MW-h with process costing \$6.00/t		\$8.40
ocean sequestration @ \$10.00/t		\$14.00
net expense/MW-h		\$6.00
removal of CO ₂ from flue gas produced at 1.4t CO ₂ /MW-h with process costing \$3.00/t		\$4.20
net expense/MW-h		\$1.80

* ave over 5 years for QLD, NSW, VIC & SA coal fired power stations

case 6: EXISTING BLACK COAL POWER STATIONS

Item	income	expense
extra electricity produced from increased efficiency by using PUTAR (based on \$41.00 /MW-h, source NEMCO)	\$16.40	
removal of CO ₂ from flue gas produced at 1.2t CO ₂ /MW-h with process costing \$6.00/t		\$7.20
ocean sequestration @ \$10.00/t		\$14.00
net expense/MW-h		\$4.80
removal of CO ₂ from flue gas produced at 1.2t CO ₂ /MW-h with process costing \$3.00/t		\$3.60
net expense/MW-h		\$1.20

case 7: IGCC (Brown Coal) & SCP PULSE COMBUSTION BOILER POWER STATIONS

Item	income	expense
extra electricity produced from increased efficiency by using SCP Pulse Combustion (based on \$41.00 /MW-h, source NEMCO)	\$20.50	
removal of CO ₂ from flue gas produced at 1.4t CO ₂ /MW-h with process costing \$6.00/t		\$8.40
ocean sequestration @ \$10.00/t		\$14.00
net expense/MW-h		\$1.90
removal of CO ₂ from flue gas produced at 1.4t CO ₂ /MW-h with process costing \$3.00/t		\$4.20
net PROFIT/MW-h	\$2.30	

case 8: NATURAL GAS SCP PULSE COMBUSTION BOILER POWER STATIONS

Item	income	expense
extra electricity produced from increased efficiency by using SCP Pulse Combustion (based on \$41.00 /MW-h, source NEMCO)	\$20.50	
removal of CO ₂ from flue gas produced at 0.7t CO ₂ /MW-h with process costing \$6.00/t		\$4.20
ocean sequestration @ \$10.00/t		\$14.00
net PROFIT/MW-h	\$2.30	
removal of CO ₂ from flue gas produced at 0.7t CO ₂ /MW-h with process costing \$3.00/t		\$2.10
net PROFIT/MW-h	\$4.40	

Permanent carbon dioxide storage in deep-sea sediments

Kurt Zenz House, Daniel P. Schrag, Charles F. Harvey, and Klaus S. Lackner

PNAS published online Aug 7, 2006;
doi:10.1073/pnas.0605318103

This information is current as of November 2006.

E-mail Alerts	This article has been cited by other articles: www.pnas.org#otherarticles
Rights & Permissions	Receive free email alerts when new articles cite this article - sign up in the box at the top right corner of the article or click here .
Reprints	To reproduce this article in part (figures, tables) or in entirety, see: www.pnas.org/misc/rightperm.shtml
	To order reprints, see: www.pnas.org/misc/reprints.shtml

Notes:

Permanent carbon dioxide storage in deep-sea sediments

Kurt Zenz House*[†], Daniel P. Schrag*, Charles F. Harvey[‡], and Klaus S. Lackner[§]

*Department of Earth and Planetary Sciences, Harvard University, Cambridge, MA 02138; [†]Department of Civil and Environmental Engineering, Massachusetts Institute of Technology, Cambridge, MA 02139; and [§]Earth Engineering Center, Columbia University, New York, NY 10027

Communicated by John P. Holdren, Harvard University, Cambridge, MA, June 27, 2006 (received for review November 10, 2005)

Stabilizing the concentration of atmospheric CO₂ may require storing enormous quantities of captured anthropogenic CO₂ in near-permanent geologic reservoirs. Because of the subsurface temperature profile of terrestrial storage sites, CO₂ stored in these reservoirs is buoyant. As a result, a portion of the injected CO₂ can escape if the reservoir is not appropriately sealed. We show that injecting CO₂ into deep-sea sediments <3,000-m water depth and a few hundred meters of sediment provides permanent geologic storage even with large geomechanical perturbations. At the high pressures and low temperatures common in deep-sea sediments, CO₂ resides in its liquid phase and can be denser than the overlying pore fluid, causing the injected CO₂ to be gravitationally stable. Additionally, CO₂ hydrate formation will impede the flow of CO₂(l) and serve as a second cap on the system. The evolution of the CO₂ plume is described qualitatively from the injection to the formation of CO₂ hydrates and finally to the dilution of the CO₂(aq) solution by diffusion. If calcareous sediments are chosen, then the dissolution of carbonate host rock by the CO₂(aq) solution will slightly increase porosity, which may cause large increases in permeability. Karst formation, however, is unlikely because total dissolution is limited to only a few percent of the rock volume. The total CO₂ storage capacity within the 200-mile economic zone of the U.S. coastline is enormous, capable of storing thousands of years of current U.S. CO₂ emissions.

climate change | CO₂ hydrates | energy | sequestration

Supplying the energy demanded by world economic growth without affecting the Earth's climate is one of the most pressing technical and economic challenges of our time. If fossil fuels, particularly coal, remain the dominant energy source of the 21st century, then stabilizing the concentration of atmospheric CO₂ will require developing the capability to capture CO₂ from the combustion of fossil fuels and store it safely away from the atmosphere (1).

Several ideas have been proposed for the long-term storage of captured anthropogenic CO₂. These proposals include: storing CO₂ in various geologic formations [e.g., oil and gas fields (2), coal beds (3), and saline aquifers (4)], injecting CO₂ into the deep ocean (5, 6), and chemically transforming CO₂ into thermodynamically stable minerals (1, 7) or bicarbonate brines (8, 9). We describe storing CO₂ in deep-sea sediments as a fourth storage option that combines beneficial elements of geologic storage, oceanic storage, and geochemical storage while addressing many of their drawbacks.

Storage of captured CO₂ in terrestrial geologic formations is a leading candidate for near-term storage. All terrestrial geologic formations, however, face a common challenge. Because of the geothermal gradient in the continental crust, the temperature at injection is always greater than the critical temperature of CO₂. Under the high pressures (10–30 MPa) and high temperatures (330–400 K) of terrestrial storage sites, supercritical CO₂ is 40–70% less dense than the surrounding pore fluid (10). This density contrast causes the buoyant CO₂ to migrate upward through any available conduit. As a result, all terrestrial storage reservoirs either must have impermeable layers (i.e., cap

rocks) or all of the injected CO₂ must become immobile as residual saturation to prevent the release of buoyant fluids. Natural-gas reservoirs have existed for millions of years, demonstrating that geologic formations can store buoyant fluids for long time periods. Over the last century, however, millions of wells have been drilled in most of the basins being considered for geologic storage, and each of these wells is a potential conduit for buoyant CO₂ to escape (11). The concern over leakage will require geologic storage sites to be monitored for centuries, and it is unclear who will be responsible for verifying the storage integrity over these time scales.

Injecting CO₂ directly into the deep ocean, where most of it will dissolve as bicarbonate, is another option for CO₂ storage (12). Deep-ocean injection can be seen as accelerating the natural oceanic uptake of CO₂, which would occur over many centuries (13). Unfortunately, because of ocean currents and local supersaturation, a large fraction of the injected CO₂ will be released to the atmosphere after a few hundred years (14). Additionally, direct ocean storage is currently unpopular because of concerns about the effects of CO₂ on marine ecosystems.[¶] Unless there is a change in the political climate, it is unlikely that direct ocean storage will be used on large scales.

Chemically transforming captured CO₂ into bicarbonate brines or thermodynamically stable minerals is a third storage option. Forming bicarbonate brines through the dissolution of calcium carbonate has been suggested as a way to neutralize carbonic acid before ocean injection (8, 9). Separately, it has been proposed that CO₂(g) can be reacted with silicate minerals to form thermodynamically stable carbonate minerals (1). Mineralization, the most stable and permanent form of CO₂ storage, is an acceleration of the natural chemical weathering cycle (15). At surface temperatures, however, the reaction kinetics are very slow, and accelerating the kinetics to industrial rates with current technology costs 3 to 10 times more than terrestrial geologic storage (16).

Results

Gravitational Stability. Because of the high compressibility of CO₂(l) relative to water, CO₂(l) becomes denser than water at high pressures and low temperatures (Fig. 1). These temperature–pressure regimes do not exist in terrestrial settings; they are, however, common in the deep ocean. When CO₂(l) is injected into the ocean at a depth of 3,000 m, it sinks, forming a lake of CO₂(l) on the seafloor (17). As previously discussed, however, ocean currents will mix the injected CO₂(l), causing a large fraction to eventually be released into the atmosphere (14). To ensure that deep ocean currents will not mix the CO₂ into shallower regions, CO₂ can be injected below the seafloor.

Conflict of interest statement: No conflicts declared.

Abbreviations: HFZ, hydrate formation zone; NBZ, negative buoyancy zone.

[†]To whom correspondence should be addressed. E-mail: khhouse@fas.harvard.edu.

[¶]Barry, J. P., Seibel, B. A. & Lovera, C., American Geophysical Union Fall Meeting, December 10–14, 2001, San Francisco, CA.

© 2006 by The National Academy of Sciences of the USA

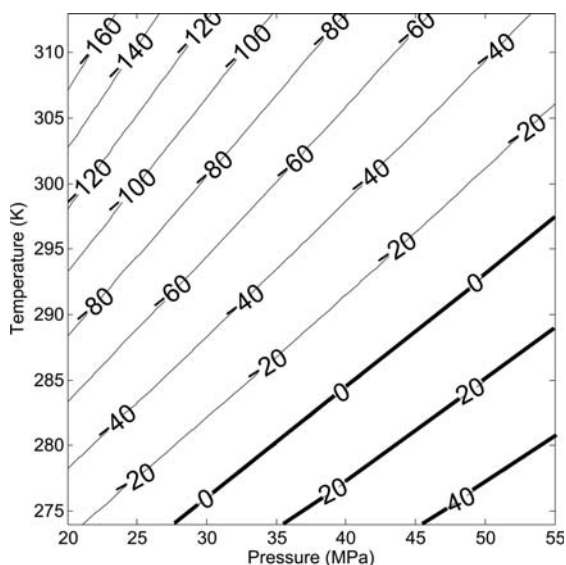


Fig. 1. Density (kg/m^3) difference between $\text{CO}_2(\text{l})$ and seawater ($1,027 \text{ kg}/\text{m}^3$) as a function of temperature and pressure (10). The bold lines indicate the pressure–temperature space of the NBZ.

Furthermore, if the seafloor depth of injection is $>3,000 \text{ m}$, then the injected CO_2 will be denser than the ambient pore fluid. The lower density pore fluid acts as a buoyancy cap on the system and ensures gravitational stability. The gravitational stability of the system in deep-sea sediments is in contrast with terrestrial geologic storage where the high pressures and high temperatures cause the injected supercritical CO_2 to be gravitationally unstable. The buoyancy cap, provided by the pore water, serves the same purpose in deep-sea sediments as a cap rock serves in terrestrial geologic formations. The buoyancy cap, however, is superior to a cap rock because conduits in a cap rock enable buoyant CO_2 to escape. In contrast, the gravitational stability provided by the buoyancy cap guarantees that fractures in the sediment column cannot serve as conduits for the CO_2 , and even large geomechanical perturbations, such as earthquakes, cannot cause the $\text{CO}_2(\text{l})$ to be released.

Storing CO_2 in deep-sea sediments was first proposed by Koide *et al.* (18) who considered storing CO_2 –clay–ash solutions and $\text{CO}_2(\text{l})$ below tens of meters of unconsolidated marine sediments. They identified three seafloor depth regimes for the storage of dissolved CO_2 : “shallow subseabed” ($<300 \text{ m}$), “deep subseabed” ($300\text{--}3,700 \text{ m}$), and “super deep subseabed” ($>3,700 \text{ m}$). In this study, we describe a different scenario than envisioned by Koide *et al.* Specifically, we consider injecting pure $\text{CO}_2(\text{l})$ below at least $3,000 \text{ m}$ of ocean and several hundred meters of marine sediment. The key aspect of our study is to inject pure $\text{CO}_2(\text{l})$ below the sediment layer where CO_2 hydrates form and below the sediment layer of less dense pore fluid. As will be discussed, the relative location of these sediment layers and the injected $\text{CO}_2(\text{l})$ ensures permanent CO_2 storage.

The geothermal gradient, which varies from $0.02^\circ\text{C}/\text{m}$ to $0.04^\circ\text{C}/\text{m}$, controls changes in the density of $\text{CO}_2(\text{l})$ injected into deep-sea sediments by expanding and contracting the mobile $\text{CO}_2(\text{l})$ until its density equals the density of the surrounding pore fluid. Given a seafloor depth of $3,500 \text{ m}$ and a geothermal gradient of $0.03^\circ\text{C}/\text{m}$, the injected $\text{CO}_2(\text{l})$ becomes neutrally buoyant at $\approx 200 \text{ m}$ below the seafloor (10). Above the sediment depth of neutral buoyancy, the $\text{CO}_2(\text{l})$ is denser than the ambient pore fluid. We refer to this range between the seafloor and the sediment depth of neutral buoyancy as the negative buoyancy zone (NBZ) (Fig. 2).

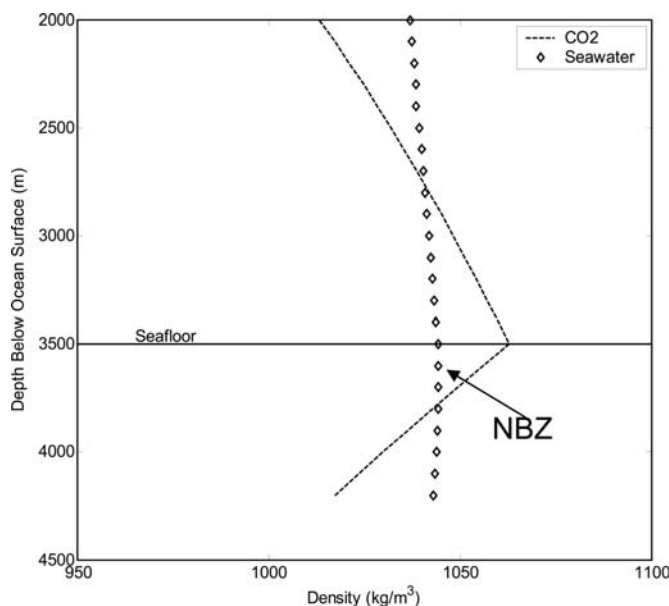


Fig. 2. Because $\text{CO}_2(\text{l})$ is more compressible than seawater, it becomes denser than seawater at $\approx 3,000 \text{ m}$ (10). Once below the seafloor, however, the geothermal gradient causes the $\text{CO}_2(\text{l})$ to expand more rapidly than seawater. Eventually, the ambient temperature becomes hot enough that $\text{CO}_2(\text{l})$ becomes less dense than the pore fluid. (Note: A linear geothermal gradient of $0.03^\circ\text{C}/\text{m}$ was assumed.)

Postinjection Chemistry and Sediment Composition. To fully describe the fate of CO_2 injected below the seafloor, the chemical reactions between CO_2 , seawater, and sediments must be considered. CO_2 that has been injected into deep-sea sediments will slowly dissolve, forming a $\text{CO}_2(\text{aq})$ solution that is denser than the surrounding pore fluid (19). At 30 MPa and 3°C , the solution becomes saturated at a $\text{CO}_2(\text{aq})$ mole fraction of $\approx 5\%$ (20). The solubility of CO_2 indicates that a given quantity of $\text{CO}_2(\text{l})$ must interact with 20 times as much pore fluid to fully dissolve. Therefore, during the injection, $\text{CO}_2(\text{l})$ is the dominant phase.

The composition of the marine sediments near the injection site will determine how the injected CO_2 interacts with the host rock. Calcareous sediments might be an attractive repository because of their relatively high permeability (21) and their tendency to react with carbonic acid. If CO_2 were injected into calcareous sediments at high pressure, then the relatively low pH of the $\text{CO}_2(\text{aq})$ solution is expected to dissolve carbonate minerals and add alkalinity to the pore fluid. The addition of alkalinity to the pore fluid will decrease the concentration of $\text{CO}_2(\text{aq})$ by shifting the carbonate equilibrium toward bicarbonate. Bicarbonate is a more permanent storage state than $\text{CO}_2(\text{aq})$ because bicarbonate cannot directly degas from solution.

The total dissolution of carbonate minerals, however, is expected to be relatively small; for a cubic meter of limestone of 50% porosity filled with CO_2 -saturated pore water in equilibrium with $30 \text{ MPa } p\text{CO}_2$, $\approx 7.5 \text{ kg}$ or 0.5% of the rock will dissolve before the pore fluid is saturated. It is important to note that the saturation calculation assumes the CO_2 -saturated pore fluid is not flowing. As described in *Long-Term Fate of CO_2 in Deep-Sea Sediments* below, both the pure $\text{CO}_2(\text{l})$ phase and the CO_2 -saturated pore fluid are expected to flow by buoyancy-driven advection. As result of that flow, certain regions in the porous media may become undersaturated in Ca^{2+} , enabling additional dissolution of the host rock.

Because CO_2 would be injected as a separate liquid phase, the host rock will not experience large fluxes of $\text{CO}_2(\text{aq})$ near the injection well. Nevertheless, host-rock dissolution may be im-

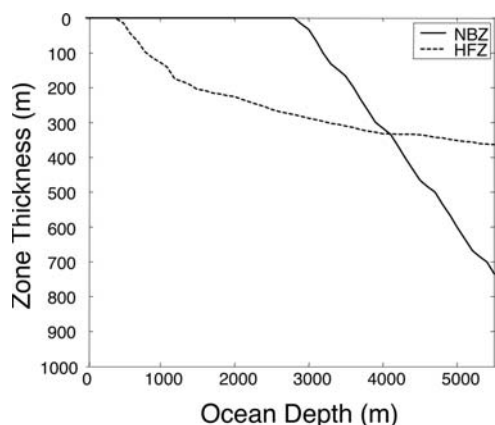


Fig. 3. The thicknesses of the HFZ and the NBZ as a function of the seafloor depth of injection. (Note: A linear geothermal gradient of 0.03°C/m was assumed.)

portant because minor increases in porosity have been shown to generate large increases in permeability (22–24). The exact relationship between porosity and permeability in carbonate sediment is highly variable (25), and further work is required to quantify whether carbonate dissolution will have a significant effect.

CO₂ Hydrate Formation. The high pressures and low temperatures necessary to compress CO₂(l) to greater density than the pore fluid are similar to the conditions necessary for CO₂ hydrates to form. CO₂ hydrates (5.75 H₂O·CO₂) are nonstoichiometric crystalline compounds that form at high pressures and low temperatures by trapping CO₂ molecules in hydrogen-bonded cages of H₂O (26). These compounds occur in a three-phase metastable equilibrium between CO₂(l), CO₂(aq), and hydrate (20).

We refer to the subsurface region with low enough temperatures and high enough pressures for hydrate formation as the hydrate formation zone (HFZ). The HFZ extends from the seafloor downward into the sediment until the temperature rises above the boundary of the hydrate stability field. A comparison of the stability conditions for CO₂ hydrates (27) with the CO₂ buoyancy-depth relationship reveals that the HFZ overlaps to a great extent with the NBZ. Although the HFZ exists in submarine sediment at seafloor depths of ≈400 m, CO₂(l) does not become denser than seawater until a seafloor depth of ≈2,900 m. Below ≈2,900 m of ocean, however, the thickness of the NBZ grows more rapidly than the thickness of the HFZ, and at seafloor depths >4,000 m, the NBZ is thicker than the HFZ (Fig. 3).

The overlap of the HFZ and the NBZ presents both implementation difficulties and storage opportunities. Hydrates are immobile crystals that clog pore spaces and impede flow. As a result, hydrate formation is expected to generate a self-forming cap that limits the migration of CO₂ and enhances storage stability. On the other hand, if the injection point is within the HFZ, then hydrate formation will decrease permeability near the injection point and may increase the energy required for injection. The optimal sediment depth of injection will depend on the relationship between depth and intrinsic permeability and on the degree to which hydrate formation affects the relative permeability of CO₂. The composition of the injection site below the HFZ may be either chalk or limestone. The intrinsic permeability of chalk and limestone ranges from 0.1 to 1,000 mD (28). If the intrinsic permeability below the HFZ is lower than the relative permeability of CO₂(l) to CO₂ hydrates, then no benefit is gained from injecting below the HFZ. Further work is needed to establish the effect of hydrate formation on permeability. We expect, however, that hydrate formation will cause

sharp reductions in the relative permeability of CO₂(l), and that locating the injection point below the HFZ will be energetically favorable to locating it within the HFZ.

When the seafloor depth is shallower than 4,000 m, the HFZ is thicker than the NBZ, and avoiding hydrate formation near the injection point requires that the CO₂(l) be injected below both the HFZ and the NBZ. CO₂(l) injected below the NBZ is buoyant at the point of injection and will rise until it reaches the bottom of the HFZ. As the CO₂(l) flows into the HFZ, it will form CO₂ hydrates, which will clog the pore space and form a cap that limits the upward migration of the remaining CO₂(l) (29). If the hydrate cap does not form an impermeable seal, then some CO₂(l) may flow within the HFZ to the bottom of the NBZ. Once that CO₂ reaches the bottom of the NBZ, it becomes neutrally buoyant and gravitationally stable. Injecting below both the HFZ and the NBZ takes advantage of both the buoyancy cap provided by the NBZ and the self-forming hydrate cap provided by the HFZ.

If CO₂ were injected into sediment below a seafloor depth of 4,000 m, where the NBZ is thicker than the HFZ, then the CO₂ would be injected below the HFZ and directly into the NBZ. In such a configuration, hydrates are unlikely to form because the CO₂(l) is expected to percolate away from the HFZ to the bottom of the NBZ where it will reside beneath both the buoyancy cap and the hydrate cap.

Discussion

Thermal Evolution of the Injected CO₂. As the CO₂ is pumped from the surface to the seafloor, heat will be transferred from the relatively warm CO₂ to the relatively cold ocean water. The temperature of the CO₂ in the pipeline as a function of depth below the ocean surface is given by the solution to the radial heat equation:

$$T(z) = T_{\text{ocean}} + (T_1 - T_{\text{ocean}})e^{-\frac{2k}{uz\Delta r r_1 \rho C_p} z}, \quad [1]$$

where k is the thermal conductivity of the pipe, ρ is the density of the fluid, r_1 is the inner radius of the pipe, Δr is the pipe thickness, T is the temperature of the CO₂ in the pipe, u_z is the velocity in the vertical direction, T_{ocean} is ocean temperature, and z is the water depth below the ocean surface. For reasonable values [$k = 50 \text{ W/(m}\cdot\text{K)}$, $r_1 = 0.25 \text{ m}$, $\Delta r = 0.1 \text{ m}$, $C_p = 2,000 \text{ J/(kg}\cdot\text{K)}$, $\rho = 1,000 \text{ kg}^3/\text{m}^3$, and $u_z = 1 \text{ m/s}$] the exponential coefficient becomes about -0.002 at $z = 3,000 \text{ m}$. Therefore, unless the pipeline is insulated, the CO₂ in the pipeline will thermally equilibrate with the ocean by the time it reaches the seafloor.

Beneath the seafloor, the sediment temperature increases by 0.02 to 0.04°C/m, but the relatively short period it takes CO₂(l) to flow through the pipeline from the seafloor to the injection point is not long enough for the CO₂(l) in the pipeline to thermally equilibrate with the sediment. Furthermore, thermal boundary layers are expected to form in the sediment around the pipe, further insulating the CO₂ once it passes beneath the seafloor. As a result, if the temperature inside the pipe is not carefully controlled, then the CO₂(l) temperature at the injection point will be several degrees colder than the pore fluid and cold enough to form CO₂ hydrates. The primary reason to inject CO₂(l) below the HFZ is to avoid hydrate formation near the injection point. Therefore, it will be necessary to carefully control the CO₂(l) temperature at the injection point by either heating the CO₂(l) in the pipeline or insulating the ocean pipeline to keep the CO₂(l) at higher temperatures.

During injection, the CO₂(l) may be colder than the surrounding pore fluid and host rock. Depending on the injection temperature, the CO₂(l) may be positively, negatively, or neutrally buoyant near the injection point. Over time, however, the CO₂(l) plume will spread, and the regions of the plume farthest

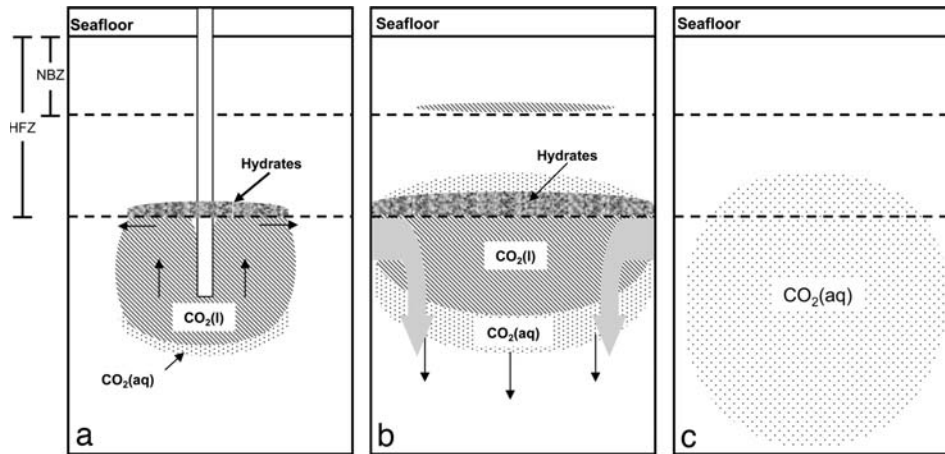


Fig. 4. The long-term evolution of the injected CO_2 . (a) On the injection time scale (≈ 1 yr), small amounts of hydrate form as the top of the plume enters the HFZ. The hydrate that forms is expected to impede the upward migration of $\text{CO}_2(\text{l})$ and force the $\text{CO}_2(\text{l})$ to flow laterally. (b) After $\approx 10^2$ years, most of the CO_2 will have reached the bottom of the HFZ, and we expect the self-forming hydrate cap will have expanded laterally and trapped substantial quantities of $\text{CO}_2(\text{l})$ below it. Simultaneously, the CO_2 -saturated pore fluid will sink away from the HFZ by buoyancy-driven advection. (c) Eventually the $\text{CO}_2(\text{l})$ and CO_2 hydrates will have dissolved and formed a $\text{CO}_2(\text{aq})$ solution. The solution will percolate through the porous matrix until it has mixed with a large enough quantity of water to become neutrally buoyant. Once the solution is neutrally buoyant, further solute migration will only occur by diffusion.

from the injection point will reach thermal equilibrium with the pore fluid. As heat is transferred from the pore fluid and the host rock to the $\text{CO}_2(\text{l})$, the $\text{CO}_2(\text{l})$ will expand and rise to the bottom of the HFZ where CO_2 hydrates begin to form.

An interesting feature of this system is that the coefficient of thermal expansion for $\text{CO}_2(\text{l})$ is high enough that, given a high enough intrinsic permeability, a typical geothermal gradient may drive some convection within the fully saturated $\text{CO}_2(\text{l})$ plume (30). The criterion for the onset of convection in a saturated porous layer subject to a vertical temperature gradient is given by the Rayleigh-Darcy number (30, 31). For the system of interest (i.e., liquid CO_2 at ≈ 30 MPa and $\approx 8^\circ\text{C}$ subject to a geothermal gradient of $\approx 0.03^\circ\text{C}/\text{m}$) the stability condition indicates that the saturated $\text{CO}_2(\text{l})$ plume is convectively unstable when the effective permeability is greater than $\approx 10^{-15} \text{ m}^2$. This stability threshold indicates that we should expect some convection within the saturated $\text{CO}_2(\text{l})$ plume because the reservoirs of interest have permeabilities in the range of 10^{-15} m^2 to 10^{-12} m^2 . The onset of convection may be important in entraining additional water into the $\text{CO}_2(\text{l})$ plume, which will cause the $\text{CO}_2(\text{l})$ to dissolve more rapidly.

Long-Term Fate of CO_2 in Deep-Sea Sediments. We expect the $\text{CO}_2(\text{l})$ injected below the seafloor to evolve in a way that ensures permanent storage (Fig. 4). Initially, the $\text{CO}_2(\text{l})$ injected below the HFZ and the NBZ will flow upward until it reaches the bottom of the HFZ. Multiphase flow in porous media is partially described by Darcy's law with the additional relative permeability parameter (K_i):

$$u_i = -\frac{\kappa K_i}{\mu_i} (\nabla P_i + \rho_i g), \quad [2]$$

where κ is the intrinsic permeability, K_i is the relative permeability of phase i , P_i is the pressure of phase i , ρ_i is the density of phase i , μ_i is the viscosity of fluid i , and g is gravity. As an order of magnitude calculation for the instantaneous flow rate of the $\text{CO}_2(\text{l})$ phase at a particular point in space and time, the driving force of the flow is the difference in density between $\text{CO}_2(\text{l})$ and seawater:

$$u_{\text{CO}_2} \approx -\frac{\kappa K_{\text{CO}_2} g}{\mu_{\text{CO}_2}} (\rho_{\text{CO}_2} - \rho_{\text{H}_2\text{O}}). \quad [3]$$

For reasonable values (e.g., $\kappa \approx 10^{-13} \text{ m}^2$, $K_{\text{CO}_2} \approx 1$, $g \approx 10 \text{ m/s}^2$, $\mu_{\text{CO}_2} \approx 10^{-4} \text{ kg}/(\text{ms})$, and $\rho_{\text{H}_2\text{O}} - \rho_{\text{CO}_2} \approx 10^2 \text{ kg}/(\text{m}^3)$), u_{CO_2} is on the order of 10^{-6} m/s ($\approx 10 \text{ m/yr}$). All of the parameters described are well constrained except for the intrinsic permeability (κ), which can vary from 10^{-12} m^2 to $\approx 10^{-15} \text{ m}^2$, resulting in a range of velocities from 10^2 m/yr to $\approx 10^{-1} \text{ m/yr}$.

Once the $\text{CO}_2(\text{l})$ reaches the bottom of the HFZ, then CO_2 hydrates will form, clogging pore channels and creating a cap of limited permeability. We expect the additional CO_2 flowing up from the injection point to become physically trapped beneath the hydrate cap and be forced to spread laterally. As the $\text{CO}_2(\text{l})$ flows laterally, the hydrate cap will grow, resulting in a larger storage area.

The hydrates that compose the self-forming cap are stable as long as they are in contact with pore fluid saturated with $\text{CO}_2(\text{aq})$. Assuming the $\text{CO}_2(\text{l})$ to $\text{CO}_2(\text{aq})$ dissolution kinetics are rapid, then the pore fluid in contact with pure $\text{CO}_2(\text{l})$ plume will be saturated in $\text{CO}_2(\text{aq})$ until the entire plume of $\text{CO}_2(\text{l})$ dissolves. Therefore, the CO_2 hydrate cap will not dissolve until the $\text{CO}_2(\text{l})$ plume has fully dissolved.

The $\text{CO}_2(\text{l})$ plume will dissolve more rapidly than expected by diffusion alone because buoyancy-driven advection will mix the $\text{CO}_2(\text{l})$ with the pore fluid. Pore fluid that becomes saturated in $\text{CO}_2(\text{aq})$ will sink because it is denser than both the $\text{CO}_2(\text{l})$ and the pristine pore fluid (19). We expect the sinking of the saturated pore fluid to entrain additional pore fluid from outside the $\text{CO}_2(\text{l})$ plume and accelerate the dissolution of $\text{CO}_2(\text{l})$ and CO_2 hydrates. Assuming a diffusion constant of $\approx 10^{-9} \text{ m}^2/\text{s}$ and a tortuosity of $\approx 10^{-1}$, diffusion sets the upper-bound on the time scale of hydrate dissolution at $\approx 10^6$ years.

It is clear, however, that buoyancy-driven advection and convection will accelerate the dissolution of the CO_2 hydrate and the downward transport of CO_2 . Once the CO_2 hydrates fully dissolve, the $\text{CO}_2(\text{aq})$ -saturated pore fluid is expected to percolate downward through the sediment column, and the $\text{CO}_2(\text{aq})$ concentration is expected to decline as the solution mixes with greater and greater volumes of water. Eventually, the buoyancy-driven advection will cease as the density difference between the

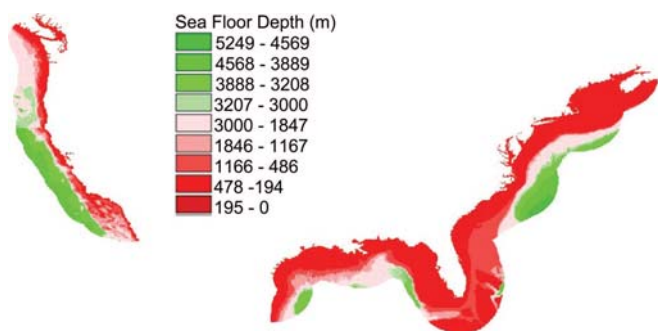


Fig. 5. More than 22% of the seafloor within the 200-mile economic zone of the U.S. coast is <3,000 m deep, which represents $>1.3 \times 10^6$ km² of potential CO₂ storage area.

CO₂(aq) solution and the pore fluid vanishes. Once that occurs, further CO₂ transport can only be accomplished by diffusion of the aqueous phase. We hope that further modeling work will determine to what degree buoyancy-driven advection and convection accelerate the hydrate dissolution and the downward transport of CO₂.

Storage Capacity. If the CO₂ storage site is 300 m thick with 50% porosity and 50% residual water, then the total annual U.S. CO₂ emissions [≈ 6 Gt of CO₂(l)] could be stored in a ≈ 80 -km² area. Fig. 5 indicates that over $\approx 22\%$ (1.3×10^6 km²) of the seafloor within the economic zone of the continental U.S. is $>3,000$ m deep (32), which represents $>10^4$ Gt of permanent CO₂(l) storage. Outside the economic zone of the United States, the total CO₂ storage capacity in deep-sea sediments is essentially unlimited.

Not all regions below 3,000 m of ocean are appropriate for CO₂ storage. Three factors will further limit the potential storage volume. First, the sediments must be thicker than the HFZ. Second, the sediments must be permeable enough to inject large quantities of liquid CO₂ at high flow rates. Third, CO₂(l) should

not be injected beneath very steep slopes as landslides may expose the CO₂(l). The thickness of the sediment is not very limiting because the majority of deep-sea sediments on the North American continental margins are thicker than the HFZ. There may, however, be mechanical difficulties associated with injecting large quantities of CO₂ into deep-sea sediments that will be discovered after further study and experimentation. Finally, a volume of pore water roughly equal to the volume of injected CO₂ will be forced up into the ocean from the sediments. The implications of forcing the pore water into the ocean must be considered.

Summary

Deep-sea sediments at high pressure and low temperature provide a virtually unlimited and permanent reservoir for carbon dioxide captured from fossil fuel combustion. When injected below the ocean floor at an ocean depth $>3,000$ m, CO₂ will remain below a layer of more buoyant pore fluid. Hydrate formation will also impede the upward flow of CO₂ as it cools along a geothermal gradient. Carbonate dissolution will play a minor role in the system and may affect permeability within the reservoir. Over time scales of thousands of years, the CO₂ will dissolve into the pore fluid, and the CO₂(aq) solution will sink until it becomes sufficiently dilute such that its density equals the density of the surrounding pore fluid. Further transport can only be accomplished by molecular diffusion over millions of years. If field experiments confirm that the system behaves as described, then the permanence guaranteed by the double cap of buoyancy and CO₂ hydrates will enable CO₂(l) to be stored without any investment in monitoring or verification technology. For these reasons, we propose that CO₂ storage in deep-sea sediments at high pressures and low temperatures be considered along with other options.

We thank John Holdren, Jeffery Bielicki, David Thompson, David Keith, Rick Murray, and Juerg Matter for assistance and advice. This work was supported by Department of Energy Grant DE-FG26-04NT-42123, the Merck Fund of the New York Community Trust, and a graduate student fellowship from the Link Foundation (to K.Z.H.).

- Lackner, K. (2002) *Annu. Rev. Energy Environ.* **27**, 193–232.
- Stevens, S., Velo, K., Gale, J. & Beecy, D. (2001) *Environ. Geosci.* **8**, 200–209.
- Gale, J. & Freund, P. (2001) *Environ. Geosci.* **8**, 210–217.
- Nordbotten, J., Celia, M. & Bachu, S. (2005) *Transport Porous Media* **58**, 339–360.
- Drange, H., Alendal, G. & Johannessen, O. M. (2001) *Geophys. Res. Lett.* **28**, 2637–2640.
- Herzog, H. (2001) *Environ. Sci. Technol.* **35**, 148A–153A.
- O’Conner, W. K., Dahlin, D. C., Turner, P. C. & Walters, R. (1999) *Carbon Dioxide Sequestration by Ex-Situ Mineral Carbonation* (Albany Research Center, Office of Fossil Energy, Department of Energy, Albany, OR), DOE/ARC-99-009.
- Rau, G. & Caldeira, K. (1999) *Energy Convers. Manage.* **40**, 1803–1813.
- Rau, G. & Caldeira, K. (2000) *Geophys. Res. Lett.* **27**, 225–228.
- Lemmon, E. W., McLinden, M. O. & Friend, D. G. (2005) in *NIST Chemistry WebBook, NIST Standard Reference Database*, eds. Linstrom, P. J. & Mallard, W. G. (National Institute of Standards and Technology, Gaithersburg, MD), Standard Reference Database no. 69.
- Nordbotten, J., Celia, M., Bachu, S. & Dahle, H. (2005) *Environ. Sci. Technol.* **39**, 602–611.
- Caldeira, K., Akai, M., Brewer, P., Chen, B., Haugan, P., Iwama, T., Johnston, P., Kheshgi, H. Q., Li, T. O., Poertner, H., et al. (2005) in *IPCC 2005: IPCC Special Report on Carbon Dioxide Capture and Storage* (Cambridge Univ. Press, Cambridge, U.K.), pp. 279–307.
- Sabine, C. L., Feely, R. A., Gruber, N., Key, R. M., Lee, K., Bullister, J. L., Wanninkhof, R., Wong, C. S., Wallace, D. W. R., Tilbrook, B., et al. (2004) *Science* **305**, 367–371.
- Jain, A. K. & Cao, L. (2005) *Geophys. Res. Lett.* **32**, L09609.
- Walker, J. C. G. (1985) *Origins Life* **116**, 117–127.
- Anderson, S. & Newell, R. (2004) *Annu. Rev. Environ. Resour.* **29**, 102–142.
- Fer, I. & Haugan, P. (2003) *Limnol. Oceanogr.* **48**, 872–883.
- Koide, H., Shindo, Y., Tazaki, Y., Iijima, M., Ito, K., Kimura, N. & Omata, K. (1997) *Energy Convers. Manage.* **38**, 253–258.
- Song, Y., Chen, B., Nishio, M. & Akai, M. (2005) *Energy* **30**, 2298–2307.
- Diamond, L. & Akiniev, N. (2003) *Fluid Phase Equilibria* **208**, 265–290.
- Spinelli, G. A., Giambalvo, E. R. & Fisher, A. T. (2004) in *Hydrogeology of the Oceanic Lithosphere*, eds. Davis, E. E. & Elderfield, H. (Cambridge Univ. Press, Cambridge, U.K.), pp. 339–369.
- Zhang, S. (1994) *J. Geophys. Res.* **99**, 741–760.
- Pruess, K. & Garcia, J. (2002) *Environ. Geol.* **42**, 282–295.
- Pape, H., Clauser, C. & Iffland, J. (1999) *Geophysics* **64**, 1447–1460.
- Enos, P. & Sawatsky, L. H. (1981) *J. Sediment. Petrol.* **51**, 961–985.
- Lee, K. M., Lee, H., Lee, J. & Kang, J. M. (2002) *Geophys. Res. Lett.* **29**, 2034.
- Bakker, R., Duessy, J. & Cathelineau, M. (1996) *Geochem. Cosmochem. Acta* **60**, 1657–1681.
- Eberli, G. & Baechle, G. (2003) *Leading Edge* **22**, 654–660.
- Koide, H. (1995) *Energy Convers. Manage.* **36**, 505–508.
- Neild, D. & Began, A. (1999) *Convection in Porous Media* (Springer, New York).
- Phillips, O. M. (1991) *Flow and Reactions in Permeable Rocks* (Cambridge Univ. Press, Cambridge, U.K.).
- National Aeronautics and Space Administration (2002) *Shuttle Radar Tomography Mission* (National Aeronautics and Space Administration, Washington, DC).

RESOURCE LETTER

Roger H. Stuewer, *Editor*

*School of Physics and Astronomy, 116 Church Street SE,
University of Minnesota, Minneapolis, Minnesota 55455*

This is one of a series of Resource Letters on different topics intended to guide college physicists, astronomers, and other scientists to some of the literature and other teaching aids that may help improve course content in specified fields. [The letter E after an item indicates elementary level or material of general interest to persons becoming informed in the field. The letter I, for intermediate level, indicates material of somewhat more specialized nature; and the letter A indicates rather specialized or advanced material.] No Resource Letter is meant to be exhaustive and complete; in time there may be more than one letter on some of the main subjects of interest. Comments on these materials as well as suggestions for future topics will be welcomed. Please send such communications to Professor Roger H. Stuewer, Editor, AAPT Resource Letters, School of Physics and Astronomy, University of Minnesota, 116 Church Street SE, Minneapolis, MN 55455; e-mail: rstuewer@physics.spa.umn.edu.

Resource letter: TA-1: Thermoacoustic engines and refrigerators

Steven L. Garrett^{a)}

Graduate Program in Acoustics, Penn State University, State College, Pennsylvania 16804

(Received 24 May 2003; accepted 27 August 2003)

不管驻波行波，能传热才是好波

*[It does not matter whether the wave is traveling or standing.
What matters is whether or not it pumps heat.]*

This Resource Letter provides an annotated guide to some of the literature pertaining to the understanding of thermoacoustic engines and refrigerators. These devices incorporate acoustical components and networks to produce mechanical power or to pump heat, or both, without the use of traditional mechanical contrivances such as pistons, linkages, and valves. To bring some order to this research and the variety of thermoacoustic engines and refrigerators produced over the past two decades, these devices also are classified as stack-based and regenerator-based. The background and motivation for this organizational structure is provided in the introduction. © 2004 American Association of Physics Teachers.

[DOI: 10.1119/1.1621034]

I. INTRODUCTION

The term “thermoacoustics” was introduced by Nikolaus Rott, who claimed that “its meaning is rather self-explanatory” [Ref. 3]. In the literal sense, Rott’s claim is entirely justified, since the field is concerned with transformations between thermal and acoustical energy. But in the early 1980s, a small group of researchers headed by John Wheatley, working at Los Alamos National Laboratory, started trying to exploit thermoacoustic concepts to create devices that would produce useful refrigeration or useful work. Over the subsequent two decades, the meaning of “thermoacoustics” has expanded to encompass the design of heat engines and refrigerators that exploit gas inertia, compliance, and resistance to create passive acoustical-phasing mechanisms. These acoustical networks and resonators substitute for pistons, flywheels, and linkages used in traditional heat engines produced since the early 18th century, when Thomas Newcomen and James Watt built engines to harness the power of steam to pump water out of mines. Those me-

chanical contrivances have remained in use to the present-day in internal-combustion engines and in vapor-compression refrigeration machines.

Thermoacoustics is still evolving rapidly. This Resource Letter is intended to provide an annotated guide to some of the most important and useful literature available to students and researchers. To orient readers and to impose some useful order on the hundreds of articles published to date, I have organized them into various categories. Some are self-explanatory, such as textbooks and review articles. But to create a meaningful organizational structure for the plethora of thermoacoustic devices and components (e.g., stacks, regenerators, resonators, transducers, heat exchangers, etc.) that have been developed thus far, the reader should be aware of a rather simple classification system based on whether the porous solid medium used to exchange heat with the working fluid (usually a gas) is a “stack” or a “regenerator.” I will classify thermoacoustic devices as engines (prime movers) or refrigerators (heat pumps), but also as standing-wave stack-based devices or traveling-wave (acoustic-Stirling or pulse-tube) regenerator-based devices.

^{a)}Electronic mail: sxg185@psu.edu

The four-category classification matrix is shown below:

	Engine (prime mover)	Refrigerator (heat pump)
Stack-based (standing-wave)		
Regenerator-based (traveling-wave)		

This scheme encompasses most cases, although some interesting hybrid thermoacoustic devices have been built that incorporate both an engine and a heat pump in the same resonator to produce a heat-driven refrigerator with no moving parts [Refs. 12, 14, 46, 94, 95 and 102]. Similarly, a new thermoacoustic heat engine has been developed that is designed to produce 1 MW of acoustic power by incorporating one stack-based prime mover to generate sound spontaneously that is subsequently amplified by two regenerator-based traveling-wave engines [Ref. 15].

I have intentionally omitted a large body of work that might also be classified as thermoacoustic. This includes pulse-combustion furnaces and a variety of economically and technologically important heat-driven oscillatory instabilities that occur in jet engines, rocket motors, and furnaces [Ref. 19].

I now elaborate on this choice of nomenclature and the resultant taxonomy for thermoacoustic engines and refrigerators as I have chosen to define them.

A. Engines and refrigerators

Cyclic thermodynamic devices are divided into two categories: engines (or prime movers) and refrigerators (or heat pumps). An engine absorbs heat at a high temperature and exhausts less heat at a lower temperature while producing work as an output. A refrigerator or heat pump absorbs heat at a low temperature and requires the input of mechanical work to exhaust more heat to a higher temperature. The only difference between a heat pump and a refrigerator is whether the purpose of the device is to cool some load or heat some load by taking the heat from a lower-temperature source (e.g., the air outside or the ground) and use the exhaust heat to warm that load (e.g., heat the air in your house).

B. Stacks and regenerators

Nearly all thermoacoustic devices employ a working fluid and some “second thermodynamic medium” that is typically a porous solid occupying less than 10% of the overall device volume. The pores or channels in the solid that contain the working fluid have a characteristic linear dimension that can be quantified by an hydraulic radius, r_h , of a typical pore or channel. The hydraulic radius is the ratio of the volume of the pores V_{gas} to the wetted area of the porous solid A_{wetted} ; $r_h = V_{\text{gas}}/A_{\text{wetted}}$. For geometrically simple regular pore geometries, the hydraulic radius can be expressed as the ratio of the pore’s cross-sectional area, A , to its perimeter Π : $r_h = A/\Pi$. For a cylindrical pore of geometrical radius a , $r_h = a/2$; for parallel plates with uniform gaps between plates of $2y_0$, $r_h = y_0$.

The linear dimension that characterizes diffusive heat transfer between the acoustically oscillating working fluid and the solid pore material, at an angular acoustic frequency

$\omega = 2\pi f$, is the thermal penetration depth, $\delta_\kappa = (2\kappa/\rho c_p \omega)^{1/2}$; where κ is the thermal conductivity of the working fluid within the pore, ρ is the fluid density, and c_p is the fluid’s constant-pressure (isobaric) specific heat per unit mass. This characteristic exponential length scale is related to the distance over which heat can diffuse during a time that is related to the acoustic period, $T = 2\pi/\omega$, of the acoustic oscillation. Useful animations showing the temperature profile of acoustically oscillating gas in contact with an isothermal solid boundary can be found at the Los Alamos National Lab Thermoacoustic Home Page [Ref. 25].

A similar exponential length that characterizes the thickness of the viscous boundary layer for oscillatory flow parallel to a solid surface is the viscous penetration depth, $\delta_\nu = (2\nu/\omega)^{1/2}$. The kinematic viscosity ν is the ratio of the shear viscosity μ to the fluid density: $\nu = \mu/\rho$. The viscous penetration depth is the quantification of the old adage: “Still waters run deep” (i.e., low frequencies correspond to long penetration depths). The thermal and viscous penetration depths are related by the Prandtl number, $\sigma = (\delta_\nu/\delta_\kappa)^2$. For most gases, $\sigma \cong 2/3$, so those lengths are nearly equal, although for mixtures of a light gas (e.g., helium) and a heavy gas (e.g., xenon), the Prandtl number can be as small as 1/5 [Refs. 49 and 50].

The dimensionless ratio of hydraulic radius to thermal penetration depth is becoming known in the thermoacoustic community as the Lautrec number, $N_L = r_h/\delta_\kappa$. If $N_L \geq 1$, the porous medium is called a “stack.” If $N_L < 1$, the porous medium is called a “regenerator.” It is called the Lautrec number because it can indicate when your regenerator is “too loose.” The Lautrec number is related to both the Womersley Number, usually taken to be $\sqrt{2}(r_h/\delta_\nu) = (2/\sigma)^{1/2} N_L$ or $2\sqrt{2}(r_h/\delta_\nu) = (8/\sigma)^{1/2} N_L$, and the Valensi number, usually taken to be $4r_h^2\omega/\nu = 8r_h^2\omega/\delta_\nu^2 = (8/\sigma)N_L^2$, which are more commonly used to characterize regenerators within the Stirling cycle community.

C. Standing-wave devices using stacks

Because $N_L \geq 1$ in a stack, the pressure oscillations of the gas are intermediate between perfectly isothermal at the solid–gas boundary and nearly adiabatic at distances greater than δ_κ away from the boundary. This imperfect thermal contact between the gas and the solid introduces a phase shift between the pressure and temperature of the gas over a distance that is within a few times δ_κ of the stack. That phase shift provides a “natural” mechanism to produce the proper phasing for heat pumping along the stack. For that reason, Wheatley referred to these stack-based devices as “natural engines” [Refs. 7, 12, and 16].

Since the phasing between the acoustical oscillations of the gas and the heat transfer between the gas and stack is provided by a natural process (thermal diffusion), stack-based thermoacoustic engines will oscillate spontaneously if a sufficiently large thermal gradient is imposed along the stack. Operation of a stack-based thermoacoustic device requires that the pressure and displacement of a parcel of oscillating gas within the stack be primarily in phase. For that reason, stack-based devices are also called “standing-wave” engines or refrigerators. Much like the optical laser, where the electromagnetic standing wave in the laser cavity synchronizes the transfer of energy from the excited electronic states to enhance the amplitude of the electromagnetic stand-

ing wave, the acoustic standing wave can phase the exchange of heat between the working fluid and the solid stack in a way that produces an initial exponential growth in the amplitude of the standing wave [Refs. 13 and 21]. The standing wave will eventually reach steady-state amplitude that is limited by the available heat input to the stack and the losses owing to radiation, thermoviscous dissipation, and the like.

One drawback to the imperfect thermal contact between the gas and the solid material of the stack is that heat transfer over a non-zero temperature span must create entropy. Hence, even an idealized stack-based thermoacoustic device cannot achieve ideal (Carnot) thermodynamic performance, even in the inviscid limit, if power density is non-zero [Ref. 4].

Several of the articles cited in this Resource Letter provide a simple explanation of the operation of standing-wave refrigerators and heat engines using a Lagrangian approach that follows an individual parcel of gas as it oscillates along the stack while its pressure and temperature vary [Refs. 4, 6, 12, 13, 16, 17, and 26]. The computer animations at the Los Alamos National Laboratory web site [Ref. 25] are particularly enlightening.

D. Traveling-wave devices using regenerators

In 1817, the Rev. Robert Stirling patented the use of a thermal storage medium he called the “economizer” that would be used in an air-filled engine that could operate at atmospheric pressure. Today, the economizer is known as a regenerator. In principle, a heat engine incorporating a regenerator can produce ideal (Carnot) thermodynamic performance when operated in a Stirling cycle. The gas-filled pores in a regenerator are so small compared to the thermal penetration depth (i.e., $N_L < 1$) that the pressure oscillations of the gas within the pores of the regenerator are held nearly isothermal by the higher heat capacity of the porous solid. Since the heat transfer between the gas and solid takes place over a vanishingly small temperature difference, there is a nearly negligible amount of entropy created during the transfer. Of course, there may be significant viscous dissipation created by the oscillatory flow of the working fluid through such small pores.

At the end of the 1970s, Peter Ceperley realized that the gas oscillating within the regenerator of a Stirling engine was executing a cycle that had the same phasing between pressure and velocity as a traveling acoustic wave. In his classic paper [Ref. 39] and patent [Ref. 87], Ceperley showed that a traveling sound wave passing through a porous medium (steel wool) that had an externally imposed temperature gradient experienced less attenuation when the sound wave was moving in the same direction as the temperature gradient and more attenuation when it was traveling against the temperature gradient. Although Ceperley did not demonstrate “gain” in that “engine,” it was only a matter of time before the quest for Carnot performance in thermoacoustic devices led to a class of regenerator-based thermoacoustic devices. Unlike the stack-based devices that operate in a standing-wave sound field, regenerator-based devices need a more complicated acoustic network to provide the proper traveling-wave phasing between pressure and gas velocity within the regenerator, while also providing a favorable ratio of pressure oscillation amplitudes in the regenerator-to-flow velocity amplitude through the regenerator (acoustic impedance).

The mechanical power produced by a regenerator in an engine or the cooling power absorbed by the regenerator in a

refrigerator (heat pump) is nearly equal to the acoustic power flow through the regenerator [Ref. 2]. The acoustic power is proportional to the product of the in phase components of the pressure and velocity of the gas oscillations within the regenerator. Since the regenerator pores are small, high gas velocities in those pores lead to large viscous dissipation. Hence, for a regenerator-based device to perform efficiently, and produce the power density required for a given application, it is advantageous to increase the magnitude of the pressure oscillations and reduce the magnitude of the velocity oscillations (i.e., increase the acoustic impedance), while maintaining the magnitude of their product (i.e., the power).

This situation is analogous to long-distance electrical-power transmission. Dissipation is due to the electrical resistance in the conductors that produces Joule heating (I^2R) losses. For a given power-transmission requirement, it is advantageous to increase the transmission voltage and reduce the current, while maintaining the in-phase product of current and voltage (hence the transmitted electrical power). The regenerator-based thermoacoustic device produced thus far will generally be more complicated than a stack-based standing-wave device, since they must include a passive acoustical network to provide the proper phasing and higher acoustic impedance than a pure traveling wave to optimize the efficiency of the regenerator.

II. GENERAL REFERENCES

A. Textbooks

1. **Fundamental Thermoacoustics**, A. Tominaga (Uchida Rokakuho, Toyko, 1998); ISBN 4-7536-5079-0 C3042. (In Japanese.) This textbook appears to be an elaboration of the relaxation-time approach that Tominaga describes in English in his review article in *Cryogenics* (Ref. 5). The text does not appear to address component design, instrumentation, or other experimental issues, but does discuss Tominaga’s computer code, THERMOACOUSTICA. (A)
2. **Thermoacoustics: A Unifying Perspective for Some Engines and Refrigerators**, G. W. Swift (Acoustical Society of America, New York, 2002); ISBN 0-7354-0065-2. This textbook provides a complete introduction to thermoacoustics that treats stack-based, regenerator-based, and pulse-tube devices (see Ref. 8) on an equal footing (hence the “unifying perspective”). In addition to a systematic development of thermoacoustic theory, two background chapters on oscillations and waves, and ideal-gas thermodynamics and heat transport, are provided along with two more chapters describing components and experimental techniques. The text also includes a CD-ROM that has computer animations, a working copy of the DELTAE thermoacoustics software (Ver. 5.1) for IBMs and Macs, and a 200-page software manual in searchable PDF format. Each chapter concludes with problems and the text includes 170 references. A detailed review of this textbook is available in the *Journal of the Acoustical Society of America* **113** (5), 2379–2381 (2003). (I)

B. Review articles

3. “Thermoacoustics,” Nikolaus Rott [*Adv. Appl. Mech.* **20**, 135–175 (1980)]. This article summarizes Rott’s theory of heat-driven acoustic oscillations and streaming developed through a series of articles published in *Z. Angew. Math. Phys.* starting in 1969. That work provided the theoretical foundation for the growth of thermoacoustics that started shortly after the publication of Rott’s review. (A)
4. “Thermoacoustic engines,” G. W. Swift, *J. Acoust. Soc. Am.* **84** (4), 1145–1180 (1988). This was the first attempt to provide a comprehensive picture of thermoacoustic devices, including a short history, a coherent development of the theory, and presentation of experimental results, with discussions of components such as heat exchangers, resonators, and transducers. Its focus is primarily on stack-based engines and refrigerators, but Swift does relate these to both Stirling engines and pulse-tube refrigerators. (A)

5. "Thermodynamic aspects of thermoacoustic theory," A. Tominaga, *Cryogenics* **35** (7), 427–440 (1995). Theoretical development that treats the thermoviscous functions using a relaxation-time formalism. (A)
6. "Thermoacoustic engines and refrigerators," G. W. Swift, in *Encyclopedia of Applied Physics* Vol. 21 (Wiley-VCH, Weinheim, 1997), pp. 245–264. This is a condensed and simplified version of Swift's 1988 review (Ref. 4) that is limited to stack-based devices. (I)
7. "Intrinsically irreversible or natural engines," J. C. Wheatley, in *Frontiers in Physical Acoustics*, Proceedings of the E. Fermi Summer School, Corso XCIII (Soc. Italiana di Fisica, Bologna, Italy, 1986), pp. 395–475. Summer school lectures with a mix of "conventional" stack-based devices and some unique extensions to magnetic systems and coupled nonlinear oscillators. (A)
8. "A review of pulse tube refrigeration," Ray Radebaugh, in *Advances in Cryogenic Engineering* **35**, edited by R. W. Fast (Plenum Press, New York, 1990), pp. 1191–1205. Pulse tube refrigerators are a class of regenerator-based devices that are attractive at cryogenic temperatures. They employ a dissipative acoustic network to provide the proper phasing of pressure and velocity through the regenerator. (I)
9. "Thermodynamical aspects of pulse tubes," A. T. A. M. de Waele, P. P. Steijaert, and J. Gijzen, *Cryogenics* **37**, 313–324 (1995). This is the first part of a two-part review (Ref. 10) of orifice pulse tube refrigerators. (A)
10. "Thermodynamical aspects of pulse tubes. II," A. T. A. M. de Waele, P. P. Steijaert, and J. J. Koning, *Cryogenics* **37**, 313–324 (1995). This is the second part of a two-part review (Ref. 9) of orifice pulse tube refrigerators. (A)
11. "Similitude in thermoacoustics," J. R. Olson and G. W. Swift, *J. Acoust. Soc. Am.* **95** (3), 1405–1412 (1994). An introduction to the Buckingham Pi theorem and to the use of dimensionless groups for analysis of thermoacoustic devices. (I)

III. POPULARIZATIONS

A. Articles

12. "The natural heat engine," J. C. Wheatley, G. W. Swift, and A. Migliori, *Los Alamos Science*, No. 14 (Fall, 1986), pp. 2–47. A very readable and well-illustrated introduction focused mainly on stack-based thermoacoustics, but with a useful introduction to the Stirling and Malone cycles. Included are descriptions and photographs of the first electrically driven stack-based refrigerator, the first dual-stack, heat-driven thermoacoustic refrigerator (the "beer cooler"), a stack-based liquid metal thermoacoustic prime mover that generates electricity using a magnetohydrodynamic transducer, the "dodeconator," and other historic gems. The entire issue is dedicated to the memory of John Wheatley (1927–1986) and concludes with an extremely affectionate 15-page discussion of his amazing career including excellent photographs. (E)
13. "The power of sound," S. L. Garrett and S. Backhaus, *Am. Sci.* **88** (6), 516–525 (2000). Also available at the *American Scientist* magazine web site: <http://www.americanscientist.org/articles/00articles/Garrett.html>. This article provides an introduction to both stack-based and regenerator-based thermoacoustic principles utilizing sketches to describe heat pumping without equations. (E)
14. "Thermoacoustics for liquefaction of natural gas," G. W. Swift and J. J. Wollan, *GasTIPS* **8** (6), 21–26 (Fall, 2002). Also available at the Los Alamos National Laboratory Thermoacoustics Home Page: www.lanl.gov/thermoacoustics/Pubs/GasTIPS.pdf. Describes heat-driven thermoacoustic engines used to provide pressure waves that drive thermoacoustic pulse-tube refrigerators to liquefy natural gas. Very nice color photos of some impressive apparatus that give meaning to the Freudian term "resonator envy." (E)
15. "New varieties of thermoacoustic engines," S. Backhaus and G. W. Swift, Proceedings of the Ninth International Congress on Sound and Vibration, Orlando, FL, 2002. Also available at the Los Alamos National Laboratory Thermoacoustics Home Page: www.lanl.gov/thermoacoustics/Pubs/ICSV9.pdf. Nice overview, but the highlight is the first published description of the Cascade thermoacoustic engine that uses a stack-based engine to "seed" two regenerator-based thermoacoustic traveling-wave amplifiers. (E)

16. "Natural engines," J. Wheatley and A. Cox, *Phy. Today* **38** (8), 50–57 (1985). An early introduction to stack-based devices with speculation on application of thermoacoustically-driven variability in stars. (E)
17. "Thermoacoustic engines and refrigerators," G. W. Swift, *Phy. Today* **48** (7), 22–28 (1995). An introduction to stack-based thermoacoustic devices that focused on early attempts to produce commercially viable prototypes. (E)
18. "Reinventing the engine," S. L. Garrett, *Nature (London)* **399**, 303–305 (1999). An attempt to provide context and a simple explanation of the breakthrough regenerator-based Backhaus/Swift thermoacoustic engine of Refs. 36 and 37. (E)
19. "Thermoacoustics," G. W. Swift, *McGraw-Hill Encyclopedia of Science and Technology*, 9th ed. (McGraw-Hill, New York, 2002), Vol. 18, pp. 353–335. (E)

B. Demonstration devices, kits, and computer animation web sites

20. "Understanding some simple phenomena in thermoacoustics with applications to acoustical heat engines," J. C. Wheatley, T. Hofler, G. W. Swift, and A. Migliori, *Am. J. Phys.* **53** (2), 147–162 (1985). A pedagogical article that mixes history, theory, and simple experiments. Provides scale drawing for a "thermoacoustic couple" and the original "Hofler Tube" thermoacoustic sound source that used liquid nitrogen to produce the required temperature gradient. (I)
21. "Build an 'acoustic laser,'" S. L. Garrett and R.-L. Chen, *Echoes* **10** (3), 4–5 (2000). Describes a simple thermoacoustic prime mover in a test tube made with heater wire and a ceramic stack shown in Fig. 3 of Ref. 13. Provides information for obtaining stack material. (E)
22. "A optimized miniature Hofler tube," T. J. Hofler and J. A. Adeff, *Acoust. Res. Lett. Online* **2** (1), 37–42 (2001). A heat-driven thermoacoustic sound source using flame heating is coupled to a horn to provide sound pressure levels as high as 149 dB_{SPL} at 930 Hz. Wear hearing protection! (E)
23. "Tabletop thermoacoustic refrigerator for demonstrations," D. A. Russell and P. Weibull, *Am. J. Phys.* **70** (12), 1231–1233 (2002). A nice and inexpensive demonstration refrigerator using a 4 in. loudspeaker and 35-mm film for the stack is described. No heat exchangers are used, yet they get the cold end of the stack to drop to 29 °F (−2 °C) after 10 min. (E)
24. "A simplified thermoacoustic engine demonstration," A. Jeromen, *Am. J. Phys.* **71** (5), 469–499 (2003). A thermoacoustic sound source (Hofler Tube, Refs. 20 and 22) using liquid nitrogen to provide the required temperature gradient. Not nearly as simple as the electrically heated "acoustic laser" above (Ref. 21). (E)
25. "LANL Thermoacoustics Animations," <http://www.lanl.gov/thermoacoustics/movies.html>. There are a wonderful series of acoustically accurate animations available on the "Thermoacoustics Home Page," maintained by Los Alamos National Laboratory. (This "home page" also includes links to other useful thermoacoustic web sites.) The animations include both stack-based and regenerator-based thermoacoustic devices as well as some fundamental acoustics covering standing and traveling waves and thermoviscous boundary effects. (Also available on the CD-ROM that accompanies Ref. 2.) (I)

IV. COMPLETE THERMOACOUSTIC DEVICES

A. Stack-based (standing-wave) refrigerators and heat pumps

26. "Thermoacoustic refrigerator for space applications," S. L. Garrett, J. A. Adeff, and T. J. Hofler, *J. Thermophys. Heat Transfer* **7** (4), 595–599 (1993). Describes a loudspeaker-driven thermoacoustic refrigerator that was launched on the Space Shuttle *Discovery* (STS-42). (E)
27. "Performance measurements on a thermoacoustic refrigerator at high amplitudes," M. E. Poese and S. L. Garrett, *J. Acoust. Soc. Am.* **107** (5), Pt. 1, 2480–2486 (2000). Simple theory suggests that cooling power increases with the square of acoustic pressure amplitude. This paper reports measurements that show deviation from that simple model at higher acoustic amplitudes in the same device described in Ref. 26. (I)
28. "The optimal stack spacing for thermoacoustic refrigeration," M. E. H. Tijani, J. C. H. Zeegers, and A. T. A. M. de Waele, *J. Acoust. Soc.*

Am. **112** (1), 128–133 (2002). Although the term “optimal” is ambiguous (highest efficiency, highest power density?) this article presents an experimental study of stacks of different spacing using a loudspeaker-driven thermoacoustic refrigerator. (I)

29. “Cyclic thermoacoustics with open flow,” R. S. Reid, W. C. Ward, and G. W. Swift, *Phys. Rev. Lett.* **80** (21), 4617–4620 (1998). A refrigerator with two stacks, two loudspeakers, and superimposed steady flow. (I)
30. “Experiments with a flow-through thermoacoustic refrigerator,” R. S. Reid and G. W. Swift, *J. Acoust. Soc. Am.* **108** (6), 2835–2842 (2000). More detail on the refrigerator with two stacks, two loudspeakers, and superimposed steady flow (Ref. 28). (I)
31. “Condensation in a steady-flow thermoacoustic refrigerator,” R. A. Hiller and G. W. Swift, *J. Acoust. Soc. Am.* **108** (4), 1521–1527 (2000). Experimental study of “wet wall” thermoacoustics (Refs. 65 and 66) using the Reid/Swift flow-through refrigerator (Ref. 29 and 30). (I)

B. Stack-based (standing-wave) engines and prime movers

32. “Analysis and performance of a large thermoacoustic engine,” G. W. Swift, *J. Acoust. Soc. Am.* **92** (3), 1551–1563 (1992). This is an excellent pedagogical article that describes the theory, construction, and operation of a 5-in.-diam electrically heated engine. (It may have been “large” in its day, but is now dwarfed by later Swift creations, such as those shown in Refs. 14 and 15.) (I)
33. “A liquid-sodium thermoacoustic engine,” G. W. Swift, *Appl. Phys. Lett.* **53**, 355–357 (1988). Liquid metals have very low Prandtl numbers, making them attractive for stack-based thermoacoustics if you are willing to work with molten metal and make your stack out of molybdenum. See Ref. 77 for the magnetohydrodynamic transducer used to extract electrical power. (E)
34. “Solar/heat driven thermoacoustic engine,” R-L. Chen and S. L. Garrett, *Proceedings of the 16th International Congress on Acoustics and 135th Meeting of the Acoustical Society of America*, edited by P. K. Kuhl and L. A. Crum (Acoustical Society of America, New York, 1998), Vol. II, pp. 813–814. Construction and performance of a solar-powered thermoacoustic engine is described. (E)
35. “Radiation from a submerged thermoacoustic source,” T. B. Gabrielson, *J. Acoust. Soc. Am.* **90** (5), 2628–2636 (1992). Coupling of a gas-filled, stack-based thermoacoustic resonator to water (see also Ref. 98). (I)
36. “Standing wave analysis of a thermoacoustic prime mover below onset of self-oscillations,” A. A. Atchley, *J. Acoust. Soc. Am.* **92** (5), 2907–2914 (1992). An interesting study of thermoacoustic engine performance prior to onset of self-maintained oscillations. (I)
37. “Radial wave thermoacoustic engines: Theory and examples for refrigerators and high-gain narrow-bandwidth photoacoustic spectrometers,” W. P. Arnott, J. A. Lightfoot, R. Raspet, and H. Moosmüller, *J. Acoust. Soc. Am.* **99** (5), 2652–2662 (1999). Theoretical study of stack-based devices in a cylindrical resonator geometry. (I)
38. “Experimental study of a radial mode thermoacoustic prime mover,” J. A. Lightfoot, W. Pat Arnott, H. E. Bass, and R. Raspet, *J. Acoust. Soc. Am.* **105** (2), 734–745 (1996). The device did not achieve onset owing to poor heat exchangers, but it was an interesting attempt. (I)

C. Regenerator-based (traveling-wave) engines and prime movers

39. “A pistonless Stirling engine—The traveling wave heat engine,” P. H. Ceperley, *J. Acoust. Soc. Am.* **66** (5), 1508–1513 (1979). The paper that stimulated interest in using sound to build engines and refrigerators in which the author demonstrates that the attenuation of a propagating sound wave in a tube is different for propagation with and against the temperature gradient imposed on a porous medium (steel wool). (E)
40. “Traveling wave thermoacoustic engine in a looped tube,” T. Yazaki, A. Iwata, T. Maekawa, and A. Tominaga, *Phys. Rev. Lett.* **81** (15), 3128–3131 (1998). A stack-based traveling-wave amplifier is described. (I)
41. “A thermoacoustic Stirling heat engine,” S. Backhaus and G. W. Swift, *Nature (London)* **399**, 335–338 (1999). The “breakthrough”

article that describes an acoustic heat engine that achieved the efficiency of a gasoline-powered engine but required no moving parts. (I)

42. “A thermoacoustic Stirling heat engine: Detailed study,” S. Backhaus and G. W. Swift, *J. Acoust. Soc. Am.* **107** (6), 3148–3166 (2000). Detailed follow-up to the *Nature* paper cited above. This provides a very pedagogical presentation that includes two levels of theory, as well as a complete description of their “jet pump,” and a thorough analysis of the energy flow at two operating points. (I)

D. Regenerator-based (traveling-wave) refrigerators and heat pumps

43. “Acoustic recovery of lost power in pulse tube refrigerators,” G. W. Swift, D. L. Gardner, and S. Backhaus, *J. Acoust. Soc. Am.* **105** (2), 711–724 (1999). An “acoustic network” is used to “recycle” the acoustic power leaving the regenerator of a pulse tube to improve the efficiency of a refrigerator. (I)
44. “Use of inertance in orifice pulse tube refrigerators,” D. L. Gardner and G. W. Swift, *Cryogenics* **37** (2), 117–121 (1997). Addition of an acoustic inertance (mass reactance) to the resistance typically used in a pulse tube refrigerator improves performance. (I)
45. “A pulse-tube cryocooler for telecommunications applications,” J. L. Martin, J. A. Corey, and C. M. Martin, in *Cryocoolers 10*, R. G. Ross, editor (Plenum, New York, 1999), pp. 181–189. Much work has been done recently in the development of orifice pulse-tube refrigerators (OPTRs), but most have been developed by industry and public disclosure of their details are rare. This article is an exception.

E. Hybrids

46. “Design and construction of a solar-powered, thermoacoustically driven thermoacoustic refrigerator,” J. A. Adeff and T. J. Hofer, *J. Acoust. Soc. Am.* **107** (6), L37–L42 (2000). Describes apparatus and results. (E)
47. “Thermoacoustic natural gas liquefier,” G. W. Swift in *Proceedings of the Department of Energy Natural Gas Conference* (Houston, TX, March 1997). This article is more easily available on the web at http://www.netl.doe.gov/publications/proceedings/97/97ng/ng97_pdf/NG7-1.PDF A standing-wave engine heated by a natural-gas burner creates thermoacoustic oscillations that power a pulse-tube cryocooler to liquefy the remaining natural gas without any moving parts. (E)

V. THERMOACOUSTIC COMPONENTS

A. Inert-gas mixtures

48. “Prandtl number and thermoacoustic refrigerators,” M. E. H. Tijani, J. C. H. Zeegers, and A. T. A. M. de Waele, *J. Acoust. Soc. Am.* **112** (1), 134–143 (2002). An experimental study of the performance of a loudspeaker-driven thermoacoustic refrigerator using different mixtures of inert gases. (Also see Ref. 24 for other measurements with this same refrigerator.) (I)
49. “Estimation of Prandtl numbers in binary mixtures of helium and other noble gases,” F. W. Jacobbe, *J. Acoust. Soc. Am.* **96** (6), 3568–3680 (1994). References 26 and 48 have shown that a decrease in Prandtl number improves the efficiency of stack-based devices. This theoretical paper calculates the reduction in Prandtl number produced by mixing a heavier inert gas with helium. (I)
50. “Working gases in thermoacoustic engines,” J. R. Belcher, W. V. Slaton, R. Raspet, H. E. Bass, and J. Lightfoot, *J. Acoust. Soc. Am.* **105** (5), 2677–2684 (1999). This paper includes measurements and extends Ref. 49 to include air and SF₆. (I)
51. “Acoustic measurements in gases,” M. R. Moldover, K. A. Gillis, J. J. Hurly, J. B. Mehl, and J. Wilhelm, in *Modern Acoustical Techniques for the Measurement of Mechanical Properties*, edited by M. Levy, H. E. Bass, and R. Stern, *Experimental Methods in Physical Sciences* Vol. 39 (Academic, New York, 2001), pp. 377–427. Although this is not an article on thermoacoustics, it does present a wonderful method for measurement of the Prandtl number of gas mixtures in Sec. 10.4.2. These authors from the National Institutes for Standards and Technology are also responsible for an acoustic determination of the Universal Gas Constant that is currently the most accurate determination (1.7 ppm) of that product of Boltzmann’s constant and Avogadro’s number.

52. "Thermoacoustic efficiency of thermoacoustic mixture separation," D. Geller and G. W. Swift, *J. Acoust. Soc. Am.* **112** (3), 504–510 (2002). High-amplitude standing waves are used to separate gas mixtures. (A)

B. Stacks and regenerators

53. "Simple harmonic analysis of regenerators," G. W. Swift and W. C. Ward, *J. Thermophys. Heat Transfer* **10** (4), 652–662 (1996). A detailed calculation that integrates steady-flow correlations for heat transfer and drag in stacked screens over time to predict performance of regenerators in oscillating flows. (A)
54. "Fabrication and use of parallel plate regenerators in thermoacoustic engines," S. Backhaus and G. W. Swift, in Proceedings of the 36th Intersociety Energy Conversion Engineering Conference, Savannah, Georgia, 2001, pp. 453–458. Also available at the Los Alamos Thermoacoustic Home Page: <http://www.lanl.gov/thermoacoustics/Pubs/index.html>. A regenerator is created by etching alternating stainless steel plates. Test data using a thermoacoustic-Stirling (Backhaus-Swift) engine (Refs. 41 and 42) demonstrate nearly a doubling in power density and a significant increase in efficiency over the original stacked-screen regenerator. (I)
55. "Thermoacoustic streaming in a resonant channel: The time-averaged temperature distribution," A. Gopinath, N. L. Tait, and S. L. Garrett, *J. Acoust. Soc. Am.* **103** (3), 1388–1405 (1998). A dimensionless treatment of heat flow in stacks provides insights to the "bucket-brigade" model of thermoacoustic heat transport in a stack. (A)
56. "Measurements of thermoacoustic functions for single pores," L. A. Wilen, *J. Acoust. Soc. Am.* **103** (3), 1406–1412 (1998). A clever experimental apparatus is used to make direct measurements of the thermoviscous functions for single stack pores of different cross-section and screens. Beautiful data. (I)
57. "Thermoacoustic in a single pore with an applied temperature gradient," G. Petculescu and L. A. Wilen, *J. Acoust. Soc. Am.* **106** (2), 688–694 (1999). The technique of Ref. 56 is applied with temperature gradient imposed on the sample. (I)
58. "Thermoacoustic in a single pore with an applied temperature gradient," L. A. Wilen, *J. Acoust. Soc. Am.* **109** (1), 179–184 (2001). The technique of Ref. 56 is applied to measure complex compressibility of gas in reticulated vitreous carbon and foamed aluminum. Both random media behaved like parallel plates and exhibited no nonlinear effects at high amplitudes (see Ref. 59). (I)
59. "High-amplitude thermoacoustic effects in a single pore," G. Petculescu and L. A. Wilen, *J. Acoust. Soc. Am.* **109** (3), 942–948 (2001). Measurements of thermoviscous functions still conform to "linear theory" for gas displacements as large as 60% of the total stack length. (I)
60. "General formulation of thermoacoustics for stacks having arbitrarily shaped pore cross sections," W. P. Arnott, H. E. Bass, and R. Raspet, *J. Acoust. Soc. Am.* **90** (6), 3228–3237 (1991). Experts in the acoustics of porous media calculate the thermoviscous functions for internal flow in stacks with square, triangular, round, and parallel-plate cross sections. Unfortunately, their choice of the thermoviscous function, $F(\lambda)$, is different than the Rott form used by Swift in Refs. 2 and 4. (A)
61. "Thermoacoustics in pin-array stacks," G. W. Swift and R. M. Keolian, *J. Acoust. Soc. Am.* **94** (2), 941–943 (1993). Calculation of thermoviscous functions for external flow around an array of cylinders that demonstrates that external flows can produce more efficient heat pumping in some cases. (A)
62. "Thermoacoustic relaxation in a pin-array stack," M. Hayden and G. W. Swift, *J. Acoust. Soc. Am.* **105** (5), Pt. 1, 2714–2722 (1997). Measurement of thermoviscous functions are made at very low frequencies on very large pins. (I)
63. "Measurements with reticulated vitreous carbon stacks in thermoacoustic prime movers and refrigerators," J. A. Adef, T. J. Hofler, A. A. Atchley, and W. C. Moss, *J. Acoust. Soc. Am.* **104** (1), 32–38 (1998). A study of "carbon foam" functioning as a stack material in a thermoacoustic refrigerator and engine. (I)
64. "Time-average temperature distribution in a thermoacoustic stack," G. Mozurkewich, *J. Acoust. Soc. Am.* **103** (1), 380–388 (1998). Calculation of convective heat transport between gas and stack. (A)
65. "Theory of inert gas-condensing vapor thermoacoustics: Propagation equation," R. Raspet, W. V. Slaton, C. J. Hickey, and R. A. Hiller, *J. Acoust. Soc. Am.* **112** (4), 1414–1422 (2002). Calculation of sound propagation in a "wet-walled" stack including evaporation and condensation effects. (A)
66. "Theory of inert gas-condensing vapor thermoacoustics: Transport equations," W. V. Slaton, R. Raspet, C. J. Hickey, and R. A. Hiller, *J. Acoust. Soc. Am.* **112** (4), 1414–1422 (2002). Calculation of mass flux and heat transfer in a "wet-walled" stack including evaporation and condensation effects. (A)
67. "Numerical simulations of a thermoacoustic refrigerator: Unsteady adiabatic flow around the stack," A. S. Worlikar and O. M. Knio, *J. Comput. Phys.* **127**, 424–451 (1996). Nice stream-function contour plots of oscillatory gas motion with vorticity between parallel plates. (I)
68. "Numerical simulations of a thermoacoustic refrigerator: Stratified flow around the stack," A. S. Worlikar, O. M. Knio, and R. Klein, *J. Comput. Phys.* **144**, 299–324 (1996). More pretty contour plots like Ref. 67, but this time with temperature distributions and energy flow. (I)

C. Heat exchangers

69. "Thermoacoustics with idealized heat exchangers and no stack," R. S. Wakeland and R. M. Keolian, *J. Acoust. Soc. Am.* **111** (6), 2654–2664 (2002). Theoretical study of thermoacoustic heat transport between two heat exchangers, but without the intervening stack. (A)
70. "Thermoacoustic refrigerator heat exchangers: Design, analysis and fabrication," S. L. Garrett, D. K. Perkins, and A. Gopinath, in *Heat Transfer 1994*, Vol. 4, pp. 375–380, Proceedings of the tenth International Heat Transfer Conference (Brighton, UK, 1994), edited by G. F. Hewitt. Description of fluid-backed, finned heat exchangers used in a dual-stack refrigerator (see Ref. 99). Includes complete thermal-resistance model of turbulent fluid flow in the tubes, fin efficiencies, etc. (I)
71. "A model for transverse heat transfer in thermoacoustics," G. Mozurkewich, *J. Acoust. Soc. Am.* **103** (6), 3318–3326 (1998). Study of the intersection between the stack and heat exchanger based on transverse temperature distribution in Ref. 72. (A)
72. "Heat transfer from transverse tubes adjacent to a thermoacoustic stack," G. Mozurkewich, *J. Acoust. Soc. Am.* **110** (2), 841–847 (2001). Time-averaged steady-flow analysis for heat exchangers used in thermoacoustics.
73. "Influence of velocity profile nonuniformity on minor losses for flow exiting thermoacoustic heat exchangers," R. S. Wakeland and R. M. Keolian, *J. Acoust. Soc. Am.* **112** (4), 1249–1252 (2002). Calculates improved expression for nonlinear flow resistance (minor loss) owing to exit effects in heat exchangers. (I)

D. Resonators

74. "Energy dissipation in oscillating flow through straight and coiled pipes," J. R. Olson and G. W. Swift, *J. Acoust. Soc. Am.* **100** (4), Pt. 1, 2123–2131 (1996). What do you lose if you want to use a coiled resonator to save space? This article has the answer and provides a simple expression for resonator quality factor which is accurate to 0.3% for $Q > 3$ in an appendix. (I)
75. "The Huygens entrainment phenomenon and thermoacoustic engines," P. S. Spoor and G. W. Swift, *J. Acoust. Soc. Am.* **108** (2), 588–599 (2000). Mode-lock two resonators in anti-phase and cancel their vibrations. (A)
76. "Acoustic streaming in pulse tube refrigerators: Tapered pulse tubes," J. R. Olson and G. W. Swift, *Cryogenics* **37**, 969–776 (1997). A slightly tapered resonator cross section is shown to cancel acoustically driven streaming flow thus reducing convective heat leaks. (A)
77. "Nonlinear standing waves in an acoustical resonator," Y. Il'inskii, B. Lipkens, T. Lucas, T. W. Van Doren, and E. Zabolotskaya, *J. Acoust. Soc. Am.* **104** (5), 2664–2674 (1998). Shock formation in standing waves can waste energy. This article is directed toward suppression of shock formation by variation in the resonator cross section. (A)
78. "Finite amplitude standing waves in harmonic and anharmonic tubes," D. F. Gaitan and A. A. Atchley, *J. Acoust. Soc. Am.* **93** (5), 2489–2495 (1993). Measurements of shock-wave suppression in a resonator with a mid-resonator constriction. (A)
79. "Nonlinear two-dimensional model for thermoacoustic engines," M. F. Hamilton, Y. A. Ilinskii, and E. A. Zabolotskaya, *J. Acoust. Soc. Am.* **111** (5), 2076–2086 (2002). Computational algorithm for nonlinear waveform distortion as a function of resonator shape. (A)

E. Transducers and measurement techniques

80. "Use of electrodynamic drivers in thermoacoustic refrigerators," R. S. Wakeland, *J. Acoust. Soc. Am.* **107** (2), 827–832 (2000). Excellent article describing the optimization of coupling between an electrodynamic driver and a resonant thermoacoustic load. (I)
81. "Accurate acoustic power measurements with a high-intensity driver," T. Hofler, *J. Acoust. Soc. Am.* **83** (2), 777–786 (1988). Although piezoresistive microphones have replaced piezoelectrics in most applications today, the paper provides a useful introduction to measurement of $P(dV/dt)$ power from a driver and has a good discussion of phase-locked-loop frequency tracking and automatic gain control. (I)
82. "Two-sensor power measurements in lossy ducts," A. M. Fusco, W. C. Ward, and G. W. Swift, *J. Acoust. Soc. Am.* **91** (4), Pt. 1, 2229–2235 (1992). The authors extend the two-microphone intensity measurement technique to highly reactive (standing-wave) sound fields. Of equal importance, they describe a variable acoustic load that can absorb controlled amounts of acoustic power by combining a valve and surge tank. (I)
83. "A liquid-metal magnetohydrodynamic acoustic transducer," G. W. Swift, *J. Acoust. Soc. Am.* **83** (1), 350–361 (1988). Extracts current from a thermoacoustically driven, liquid-sodium-filled resonator of Ref. 33. (I)
84. "Parametrically driven variable-reluctance generator," W. Wright and G. W. Swift, *J. Acoust. Soc. Am.* **88** (2), 609–615 (1990). A novel transducer that extracts electrical power from the motion of a resonator undergoing thermoacoustically driven vibrations. (I)
85. "Measuring second-order, time-averaged pressure," B. L. Smith and G. W. Swift, *J. Acoust. Soc. Am.* **110** (2), 717–723 (2001). Identifies pitfalls and provides solutions for measurement of time-averaged pressures in acoustic resonators. A novel eight-speaker system is used to achieve high amplitudes. (I)
92. "Thermoacoustic magnetohydrodynamic electrical generator," J. C. Wheatley, G. W. Swift, and A. Migliori, US Patent No. 4,599,511 (1986). Liquid-metal-filled stack-based, standing-wave engine. (E)
93. "Acoustic cooling engine," T. J. Hofler, J. C. Wheatley, G. W. Swift, and A. Migliori, US Patent No. 4,722,201 (1988). This is the only easily accessible description of the stack-based, standing-wave refrigerator that was Tom Hofler's Ph.D. thesis project. (I)
94. "Heat-driven acoustic cooling engine having no moving parts," J. C. Wheatley, G. W. Swift, A. Migliori, and T. J. Hofler, US Patent No. 4,858,441 (1989). Combines a stack-based engine and stack-based refrigerator in one standing-wave resonator. (E)
95. "Acoustic cryocooler," G. W. Swift, R. A. Martin, and R. Radebaugh, US Patent No. 4,953,366 (1990). Heat-driven dual-stack thermoacoustic engine with a looped resonator drives a pulse-tube refrigerator producing liquid air. (I)
96. "Compact acoustic refrigerator," G. A. Bennett, US Patent No. 5,165,243 (1992). Stack-based standing-wave refrigerator that uses tapered plate spacing for cooling of electronics in an oil-exploration borehole environment. (E)
97. "Electronics package with improved thermal management by thermoacoustic heat pumping," G. M. Chrysler and D. T. Vader, US Patent No. 5,303,555 (1994). Re-entrant horn geometry for the resonator places the cold side of a stack-based thermoacoustic refrigerator in contact with a computer chip. (E)
98. "Thermoacoustic sound source," T. B. Gabrielson, US Patent No. 5,369,625 (1994). Thermoacoustic source for underwater sound generation. (I)
99. "High-power thermoacoustic refrigerator," S. L. Garrett, US Patent No. 5,647,216 (1997). Dual-stack, dual-driver standing-wave refrigerator. (I)
100. "Thermoacoustic refrigerator," W. Moss, US Patent No. 5,673,561 (1997). Uses reticulated vitreous carbon as the stack material. (E)
101. "Passive frequency stabilization of an acoustic resonator," S. L. Garrett, US Patent No. 5,857,340 (1999). Carbon granules provide selective absorption of species in a binary-gas mixture to maintain constant resonator resonance frequency in a thermoacoustic refrigerator as the temperature changes. (I)
102. "High-efficiency heat-driven acoustic cooling engine with no moving parts," T. J. Hofler, US Patent No. 5,901,556 (1999). Two stacks in two resonators joined at a velocity anti-node. (I)
103. "Torsionally resonant toroidal thermoacoustic refrigerator," S. L. Garrett, US Patent No. 5,953,921 (1999). Stack-based refrigerator driven by a torsionally oscillating toroidal resonator. Also claims a vibromechanical pump that uses the centripetal acceleration of the oscillating resonator to pump the heat exchange fluids. (I)
104. "Traveling-wave device with mass flux suppression," G. W. Swift, S. N. Backhaus, and D. L. Gardner, US Patent No. 6,032,464 (2000). Acoustic network plus a diaphragm or jet pump to suppress Gedeon streaming. (I)
105. "High-efficiency moving magnet loudspeaker," S. L. Garrett, R. M. Keolian, and R. W. M. Smith, US Patent No. 6,307,287 (2001). Mechanically resonant electrodynamic loudspeaker with metal bellows seal and mechanical springs used to drive a large standing-wave stack-based refrigerator. (I)
106. "Thermo-acoustic system," C. M. De Blok and N. A. H. J. Van Rijt, US Patent No. 6,314,740 (2001). Several clever acoustic networks are described to make regenerator-based (traveling-wave) thermoacoustic engines and refrigerators. (I)

VI. PATENT POTPOURRI

Owing to the commercial potential of thermoacoustic devices, much useful material is available in the patent literature that is not available elsewhere. The following are simply ordered by date of issue. With the exception of some patents of particular importance, preference has been given to devices that are not described elsewhere. These are very easy to access through the web site of the United States Patent and Trademark: www.uspto.gov. Also, it is easy to get an update on new patents in the same field or by the same author. (It is never a waste of time to search under G. W. Swift if you want the "latest and greatest" in thermoacoustics.)

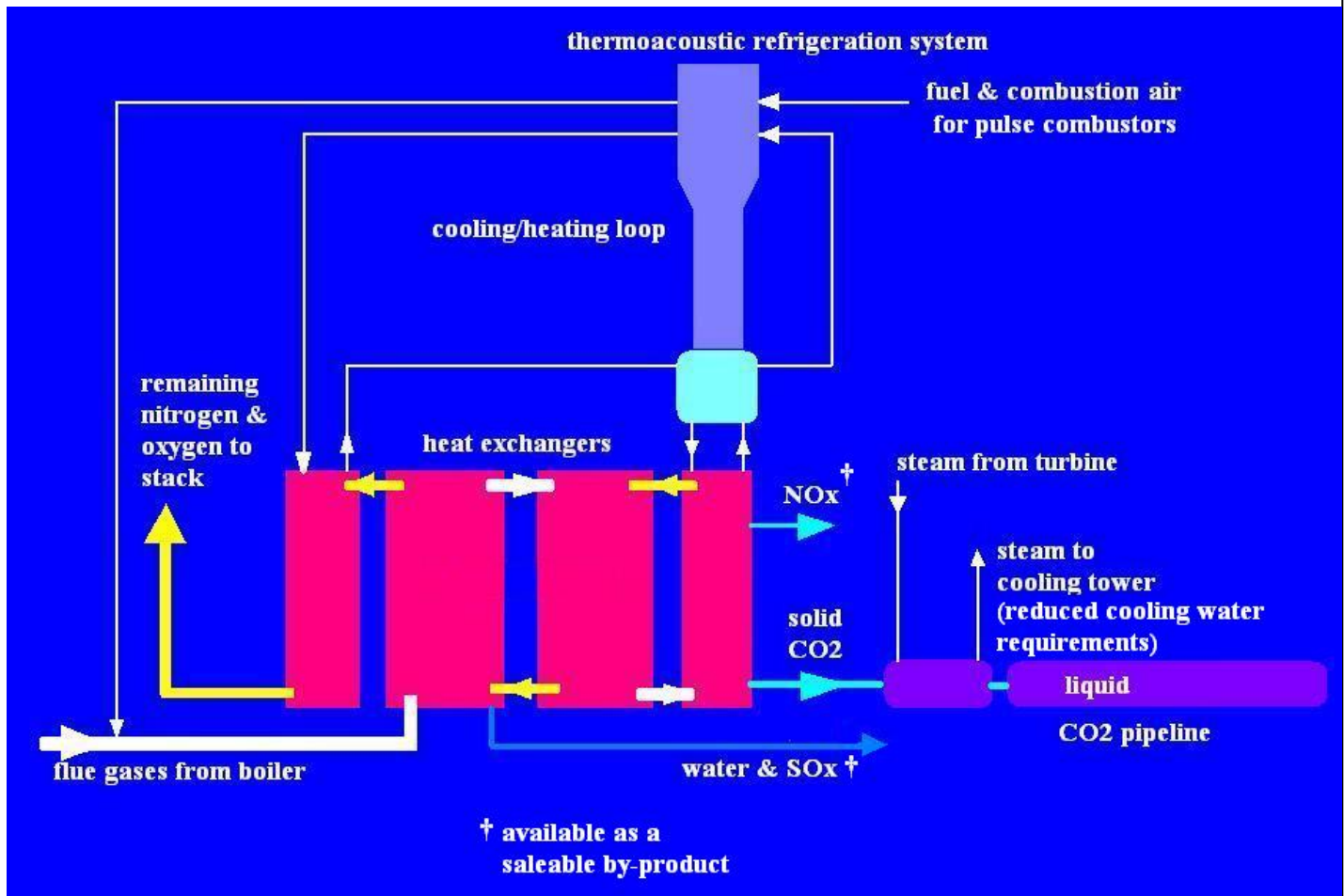
86. "Heat controlled acoustic wave system," W. A. Marrison, US Patent No. 2,836,033 (1958). This early contribution from Bell Labs describes a system to extract electricity or mechanical work from a standing-wave thermoacoustic device with heat exchangers but no stack. (E)
87. "Traveling wave heat engine," P. H. Ceperley, US Patent No. 4,114,380 (1978). The original acoustic-Stirling patent. (E)
88. "Resonant traveling wave heat engine," P. H. Ceperley, US Patent No. 4,335,517 (1982). In this improvement to his original patent (Ref. 87), Ceperley realizes that he must use "an acoustic resonant cavity to superimpose standing waves on the traveling wave of a traveling wave heat engine in order to increase the power throughput of the engine for a given level of internal losses." (I)
89. "Acoustical heat pumping engine," J. C. Wheatley, G. W. Swift, and A. Migliori, US Patent No. 4,398,398 (1983). The first Los Alamos stack-based, standing-wave refrigerator. (I)
90. "Intrinsically irreversible heat engine," J. C. Wheatley, G. W. Swift, and A. Migliori, US Patent No. 4,538,464 (1985). Follow up to Ref. 89 that provides a more general understanding of the refrigerator and heat pump.
91. "Method of measuring reactive acoustic power density in a fluid," J. C. Wheatley, G. W. Swift, and A. Migliori, US Patent No. 4,599,511 (1986). Since an acoustic standing wave will create a temperature gradient in a stack, why not measure the temperature gradient to infer the acoustic power density? (I)

ACKNOWLEDGMENTS

It should be clear from the preponderance of important articles and patents by Greg Swift that the entire field is indebted to his extraordinary insight, creativity, and generosity. I was supported by an endowment provided by the United Technologies Corporation during the writing of this Resource Letter. I am grateful to Ray Wakeland, Kevin Bastyr, and Matthew Poese, students enrolled in the Penn State Graduate Program in Acoustics, and working on theses in thermoacoustics, for collecting, copying, and organizing over 500 articles, technical reports, and patents.

Fig. 1.

100+*% REMOVAL OF CO₂ FROM INDUSTRIAL PROCESSES



The combustion products are fed into a series of heat exchangers and are cooled down by the returning remnant gases from the refrigeration process. Water, SO_x and NO_x present get condensed out of the flue gas stream as individual components, i.e. the NO_x is collected as N₂O, NO and NO₂ separately.

CO₂ is collected as a solid and fed into a series of chambers where it is allowed to pressurise and go into the liquid phase ready for transfer to a sequestration process. The pressurisation process can be assisted with steam earmarked for the condensers in power stations thus saving on cooling water requirements. Also, power station operators no longer need to keep the flue gases above 200 °C to prevent condensation in the chimney stacks and can therefore recover more heat from the fuel.

*The exiting gases now have only about 270ppm of CO₂ as opposed to around 400ppm of CO₂ in the incoming combustion air. For a 1000MW power station this amounts to \$300,000 per year in carbon credits (based on the EU price, approx. AUD 33.00) over and above what it would generate from the total removal of CO₂ from fuel.

The refrigeration processes is powered by pulse combustion. This enables a very compact and efficient “engine” at one end of the pulse tube that forms the thermo-acoustic refrigerator. Modifications to the cold end of the pulse tube further improve the efficiency of this refrigerator.

The application of this process, together with pulse combustion in the coal burning process, or the burning of natural gas, could result in greenhouse gas free electricity at, or lower than, today’s electricity prices. Capture by liquefaction of the greenhouse gases is expected to cost some AUD 3.00 per tonne.
ENDS.



Prototype 500 GPD Natural Gas Acoustic Liquefier (minus 165 degrees C) Produced by Chart at Denver, Colorado, USA.

This was a 1,600 times scale up from the laboratory model. Current target is to go to 25,000 GPD per unit, a scale up of only 50 times over the model shown.

With the scale up, efficiency was greatly improved and at 25,000 GPD the efficiency target is 90%. It is expected that this will be achieved.

For “greenhouse gases” the temperature requirement is lower at minus 85 to minus 160 degrees C.